Adv. Theor. Appl. Mech., Vol. 1, 2008, no. 3, 95 - 106

An Efficient 3D Timoshenko Beam Element with Consistent Shape Functions

Yunhua Luo

Department of Mechanical & Manufacturing Engineering
University of Manitoba, Winnipeg, R3T 5V6, Canada
luoy@cc.umanitoba.ca

Abstract

An efficient three-dimensional (3D) Timoshenko beam element is presented in this paper. First, the homogeneous Euler-Lagrangian equations governing a 3D Timoshenko beam are derived by introducing plane cross-section assumption into the kinematic description of a 3D solid continuum; then, consistent shape functions for a 3D 2-node Timoshenko beam element are constructed from the general solutions to the homogeneous Euler-Lagrangian equations. Numerical tests show that the developed 3D Timoshenko beam element is completely free from shear locking, and furthermore the performance of the element in convergence is superior to the isoparametric Timoshenko beam element with reduced integration. For the benchmark used in the test, using one of the developed beam element can produce exact solution.

Keywords: 3D Timoshenko beam, Euler-Lagrangian equation, consistent shape function

1 Introduction

Under the assumption that a plane cross-section remains plane after deformation, there are basic two categories of beam theories: Euler-Bernoulli beam and Timoshenko beam. The difference between them is whether, or not, a cross-section plane of the beam is always perpendicular to the beam axis in deformation. Experiments have demonstrated that Euler-Bernoulli assumption is more accurate for thin beams; while for a deep beam, a cross-section plane is not necessarily perpendicular to the beam axis, and shear force is a more dominant factor in the damage of material. As it is difficult to put a strict line between the two beam theories in practice, it is highly desired that the two beam theories can be unified [3, 2], both theoretically and in implementation.

Theoretically, Timoshenko beam theory is more general, and Euler-Bernoulli theory can be considered as a special case of Timoshenko assumption by enforcing the constraint condition between deflection and cross-section rotation. But in implementation, the story is different. It is well known that the conventional 2-node isoparametric Timoshenko beam element [1, 8] suffers from the so-called shear locking. Although reduced integration [12] can alleviate shear locking to some extent, the performance of the element is still not optimal. It is noticed that a very efficient 2D Timoshenko beam element was developed independently in [4, 5, 6] and in [11] at nearly the same time period and based on a very similar way, i. e. by constructing shape functions from the general solutions to the homogeneous Euler-Lagrange equations. It was further demonstrated in [6] that shear locking is an extreme case of numerical deficiency arising from neglecting inter-dependence between field functions.

In this paper, based on the work of [4, 5, 6], an efficient three-dimensional 2-node Timoshenko beam element is developed. The layout of this paper is as follows. In Section 2, the homogeneous Euler-Lagrangian equations governing a 3D Timoshenko beam is revisited based on the degeneration of a 3D solid continuum; In Section 3, consistent shape functions of a 2-node 3D Timoshenko beam element are constructed; Numerical tests are presented in Section 4 and concluding remarks are given in Section 5.

2 Homogeneous Euler-Lagrangian equations governing 3D Timoshenko beam

In this section, homogeneous Euler-Lagrangian equations governing a three-dimensional Timoshenko beam is derived from the kinematic description of a 3D solid continuum by introducing the assumption of plane cross-section of beam in deformation.

Consider a three-dimensional 2-node beam element depicted in Fig. 1. The

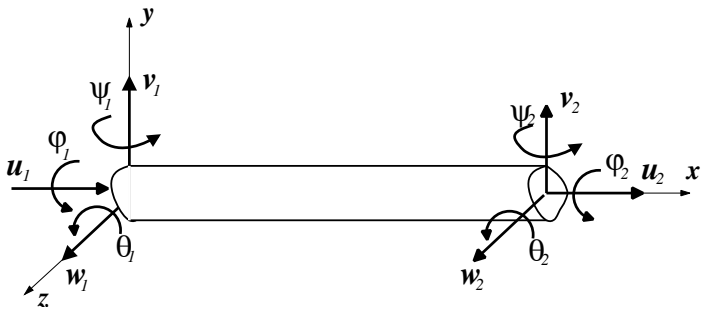

Figure 1: A 3-D 2-node beam element

element has two nodes, each node has six degrees of freedom (DOF), i.e., three translations and three rotations. There is no external force acting on the beam in between the two nodes. To describe the motion of a typical particle p in the beam, we split its motion into two parts as shown in Fig. 2, the translation

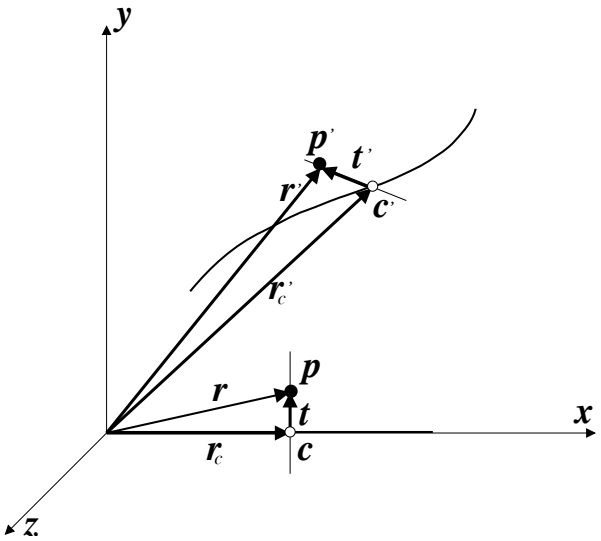

Figure 2: Kinematics of a typical particle in a 3D beam

of point c at the beam axis and the rotation of vector $\boldsymbol{t}$ defined by p and c. Vectors $\boldsymbol{t}$ and $\boldsymbol{r}_c$ are orthogonal to each other in the undeformed configuration. The motion of point c is described by three translations u_c, v_c and w_c along the three axes, respectively. According to Euler-Chasles' theorem, the rotation of vector $\boldsymbol{t}$ can be realized by a rotational operator $\boldsymbol{R}$ [9, 10], i. e.

$$\boldsymbol{t}' = \boldsymbol{R}\,\boldsymbol{t} \tag{1}$$

where

$$\boldsymbol{R} = \exp(\tilde{\boldsymbol{\Psi}}) = \boldsymbol{I}_3 + \tilde{\boldsymbol{\Psi}} + \frac{1}{2}\tilde{\boldsymbol{\Psi}}^2 + \cdots \tag{2}$$

$$\tilde{\boldsymbol{\Psi}} = \begin{bmatrix} 0 & -\theta & \psi \\ \theta & 0 & -\varphi \\ -\psi & \varphi & 0 \end{bmatrix} \tag{3}$$

φ, ψ and θ are the rotational angles of vector $\boldsymbol{t}$ around the three axes x, y and z, respectively, as shown in Fig. 2.

The position vectors of particle p before and after deformation are, respectively,

$$\begin{aligned} \boldsymbol{r} &= \boldsymbol{r}_c + \boldsymbol{t} \\ \boldsymbol{r}' &= \boldsymbol{r}_c' + \boldsymbol{t}' = \boldsymbol{r}_c' + \boldsymbol{R}\,\boldsymbol{t} \end{aligned} \tag{4}$$

So the displacement vector of p is

$$\boldsymbol{u} = \boldsymbol{r}^{'} - \boldsymbol{r} = \boldsymbol{u}_c + (\boldsymbol{R} - \boldsymbol{I}_3)\,\boldsymbol{t} \tag{5}$$

where $\boldsymbol{I}_3$ is a 3×3 unit matrix; $\boldsymbol{u} = [\ u \quad v \quad w\ ]^T$ and $\boldsymbol{u}_c = [\ u_c \quad v_c \quad w_c\ ]^T$.

If it is assumed that the rotation angles φ, ψ and θ are small, and in the Taylor series in Eq. (2), only the first two terms are retained. Therefore, the displacements of particle p in Eq. (5) are now expressed as

$$\begin{cases} u = u_c - \theta\, y + \psi\, z \\ v = v_c - \varphi\, z \\ w = w_c + \varphi\, y \end{cases} \tag{6}$$

If it is further assumed that the strains are small so that a linear strain-displacement relation can be adopted, the three non-trivial strains for a 3D beam have the following expressions

$$\begin{cases} \epsilon_{xx} = \dfrac{\partial u}{\partial x} = u_c^{'} - \theta^{'}\, y + \psi^{'}\, z \\ \epsilon_{xy} = \dfrac{\partial v}{\partial x} + \dfrac{\partial u}{\partial y} = v_c^{'} - \varphi^{'}\, z - \theta \\ \epsilon_{xz} = \dfrac{\partial w}{\partial x} + \dfrac{\partial u}{\partial z} = w_c^{'} + \varphi^{'}\, y + \psi \end{cases} \tag{7}$$

where $(\ )^{'} = \dfrac{d}{dx}$.

From now on, the subscript c is dropped, and u, v and w are now used to represent the displacements of a point at the beam axis.

Six generalized strains are introduced. They are, respectively, axial strain ($\bar{\epsilon}$), curvature in xoy plane ($\bar{\kappa}_y$), curvature in xoz plane ($\bar{\kappa}_z$), shear strains (γ_y and γ_z), and torsional rate ($\bar{\kappa}_x$),

$$\begin{cases} \bar{\epsilon} = u^{'} \\ \bar{\kappa}_y = -\theta^{'} \\ \bar{\kappa}_z = \psi^{'} \\ \bar{\gamma}_y = v^{'} - \theta \\ \bar{\gamma}_z = w^{'} + \psi \\ \bar{\kappa}_x = \varphi^{'} \end{cases} \tag{8}$$

With (8), Eq. (7) is reformed as

$$\begin{cases} \epsilon_{xx} = \bar{\epsilon} + \bar{\kappa}_y\, y + \bar{\kappa}_z\, z \\ \epsilon_{xy} = \bar{\gamma}_y - \bar{\kappa}_x\, z \\ \epsilon_{xz} = \bar{\gamma}_z + \bar{\kappa}_x\, y \end{cases} \tag{9}$$

The virtual strain energy in the beam body is calculated by

$$\begin{aligned} \delta V &= \int_{\Omega} (\sigma_{xx}\,\delta\epsilon_{xx} + \sigma_{xy}\,\delta\epsilon_{xy} + \sigma_{xz}\,\delta\epsilon_{xz})\,d\Omega \\ &= \int_{0}^{L} (N\,\delta\bar{\epsilon} + M_z\,\delta\bar{\kappa}_y + M_y\,\delta\bar{\kappa}_z + Q_y\,\delta\bar{\gamma}_y + Q_z\,\delta\bar{\gamma}_z + M_x\,\delta\bar{\kappa}_x)\,dx \end{aligned} \tag{10}$$

where L is the length of the beam element; N, M_y, M_z, Q_y, Q_z and M_x are internal forces that are conjugate, in energy, with the generalized strains, $\bar{\epsilon}$, $\bar{\kappa}_y$, $\bar{\kappa}_z$, $\bar{\gamma}_y$, $\bar{\gamma}_z$ and $\bar{\kappa}_x$, respectively,

$$\begin{cases} N = \displaystyle\int_A \sigma_{xx}\,dA = EA\,\bar{\epsilon} + EA_y\,\bar{\kappa}_y + EA_z\,\bar{\kappa}_z \\ M_z = \displaystyle\int_A \sigma_{xx}\,y\,dA = EA_y\,\bar{\epsilon} + EI_y\,\bar{\kappa}_y + EJ\,\bar{\kappa}_z \\ M_y = \displaystyle\int_A \sigma_{xx}\,z\,dA = EA_z\bar{\epsilon} + EJ\,\bar{\kappa}_y + EI_z\,\bar{\kappa}_z \\ Q_y = \displaystyle\int_A \sigma_{xy}\,dA = k\,GA\,\bar{\gamma}_y - kGA_z\,\bar{\kappa}_x \\ Q_z = \displaystyle\int_A \sigma_{xz}\,dA = k\,GA\,\bar{\gamma}_z + kGA_y\,\bar{\kappa}_x \\ M_x = \displaystyle\int_A (\sigma_{xz}\,y - \sigma_{xz}\,z)\,dA = -kGA_z\,\bar{\gamma}_y + kGA_y\,\bar{\gamma}_z + kG(I_y + I_z)\bar{\kappa}_x \end{cases} \tag{11}$$

In the above expressions, A, A_y, A_z, I_y, I_z and J are beam cross-section parameters; k is the coefficient accounting for different shapes of beam cross-section.

$$\begin{aligned} A &= \int_A dA, \qquad & J &= \int_A y\,z\,dA \\ A_y &= \int_A y\,dA, & A_z &= \int_A z\,dA \\ I_y &= \int_A y^2\,dA, & I_z &= \int_A z^2\,dA \end{aligned}$$

Equation (11) can be put in a compact form

$$\boldsymbol{p} = \boldsymbol{D}\,\boldsymbol{\rho} \tag{12}$$

in which

$$\begin{aligned} \boldsymbol{p} &= [\ N \quad M_y \quad M_z \quad Q_y \quad Q_z \quad M_x\ ]^T \\ \boldsymbol{\rho} &= [\ \bar{\epsilon} \quad \bar{\kappa}_y \quad \bar{\kappa}_z \quad \bar{\gamma}_y \quad \bar{\gamma}_z \quad \bar{\kappa}_x\ ]^T \end{aligned}$$

$$\boldsymbol{D} = \begin{bmatrix} EA & EA_y & EA_z & 0 & 0 & 0 \\ EA_y & EI_y & EJ & 0 & 0 & 0 \\ EA_z & EJ & EI_z & 0 & 0 & 0 \\ 0 & 0 & 0 & k\,GA & 0 & -kGA_z \\ 0 & 0 & 0 & 0 & k\,GA & k\,GA_y \\ 0 & 0 & 0 & -k\,GA_z & k\,GA_y & k\,G(I_y + I_z) \end{bmatrix}$$

By introducing the relations in (8) into Eq. (10), the virtual strain energy is now expressed by displacements, rotations and their derivatives,

$$\begin{aligned}\delta V &= \int_0^L \{(EA\,u^{'} - EA_y\,\theta^{'} + EA_z\,\psi^{'})\,\delta u^{'} \\ &\quad -(EA_y\,u^{'} - EI_y\,\theta^{'} + EJ\,\psi^{'})\,\delta\theta^{'} \\ &\quad +(EA_z\,u^{'} - EJ\,\theta^{'} + EI_z\,\psi^{'})\,\delta\psi^{'} \\ &\quad +[k\,GA\,(v^{'} - \theta) - k\,GA_z\,\varphi^{'}]\,(\delta v^{'} - \delta\theta) \\ &\quad +[k\,GA\,(w^{'} + \psi) + k\,GA_y\,\varphi^{'}]\,(\delta w^{'} + \delta\psi) \\ &\quad +[k\,GA_y\,(w^{'} + \psi) - k\,GA_z\,(v^{'} - \theta) + k\,G\,(I_y + I_z)\,\varphi^{'}]\,\delta\varphi^{'}\}\,dx\end{aligned} \tag{13}$$

With integrating by parts and collecting the terms with respect to δu, δv, δw, $\delta\varphi$, $\delta\psi$ and $\delta\theta$, the expression in (13) becomes

$$\begin{aligned}\delta V &= \int_0^L \{(EA\,u^{''} - EA_y\,\theta^{''} + EA_z\,\psi^{''})\,\delta u \\ &\quad +[k\,GA\,(v^{''} - \theta^{'}) - k\,GA_z\,\varphi^{''}]\,\delta v \\ &\quad +[k\,GA\,(w^{''} + \psi^{'}) + k\,GA_y\,\varphi^{''}]\,\delta w \\ &\quad +[-EA_y\,u^{''} + EI_y\theta^{''} - EJ\,\psi^{''} - k\,GA\,(v^{'} - \theta) + k\,GA_z\,\varphi^{'}]\,\delta\theta \\ &\quad +[EA_z\,u^{''} - EJ\,\theta^{''} + EI_z\,\psi^{''} + k\,GA(w^{'} + \psi) + k\,GA_y\,\varphi^{'}]\,\delta\psi \\ &\quad +[k\,GA_y\,(w^{''} + \psi^{'}) - k\,GA_z(v^{''} - \theta^{'}) + k\,G\,(I_y + I_z)]\,\delta\varphi\}\,dx + \delta V_b\end{aligned} \tag{14}$$

where $()'' = \dfrac{d^2}{dx^2}$; δV_b collects all the terms related to boundary values.

Based on the principle of virtual work, the stored strain energy is equal to the virtual work done by external forces. As it is assumed that no external force is applied on the element, and external virtual work only contributes to the inhomogeneous terms, therefore, the homogeneous Euler-Lagrangian equations are obtained as

$$\begin{cases} EA\,u^{''} - EA_y\,\theta^{''} + EA_z\,\psi^{''} = 0 \\ k\,GA\,(v^{''} - \theta^{'}) - k\,GA_z\,\varphi^{''} = 0 \\ k\,GA\,(w^{''} + \psi^{'}) + k\,GA_y\,\varphi^{''} = 0 \\ -EA_y\,u^{''} + EI_y\,\theta^{''} - EJ\,\psi^{''} - k\,GA(v^{'} - \theta) + k\,GA_z\,\varphi^{'} = 0 \\ EA_z\,u^{''} - EJ\,\theta^{''} + EI_z\,\psi^{''} + k\,GA\,(w^{'} + \psi) + k\,GA_y\,\varphi^{'} = 0 \\ k\,GA_y\,(w^{''} + \psi^{'}) - k\,GA_z\,(v^{''} - \theta^{'}) + k\,G\,(I_y + I_z)\,\varphi^{''} = 0 \end{cases} \tag{15}$$

If beam cross-section is symmetrical, or the element local coordinate axes are selected to pass through the cross-section shear center, then, $A_y = 0$, $A_z = 0$, and $J = 0$, the homogeneous Euler-Lagrangian equations in (15) are simplified

as

$$\begin{cases} EA\,u'' = 0 \\ k\,GA\,(v'' - \theta') = 0 \\ k\,GA\,(w'' + \psi') = 0 \\ EI_y\,\theta'' - k\,GA(v' - \theta) = 0 \\ EI_z\,\psi'' + k\,GA\,(w' + \psi) = 0 \\ k\,G\,(I_y + I_z)\,\varphi'' = 0 \end{cases} \tag{16}$$

3 Consistent Shape Functions and Explicit Element Stiffness Matrix

From observing the homogeneous Euler-Lagrangian equations in (15) or (16), it can be concluded that the field functions, u, v, w, θ, ψ and φ are dependent to each other, as the equations are coupled. Nevertheless, in the conventional Finite Element Method, these field functions are assumed completely independent and their variations over an element are interpolated by simple shape functions. It is demonstrated in [6, 7] that the ignorance of the inter-dependence between field functions is the fundamental reason responsible for various numerical deficiencies such as shear locking and membrane locking appeared in finite elements. An effective way to consider the inter-dependence of field functions is the use of general solutions to the homogeneous Euler-Lagrangian equations to construct element shape functions. With the use of symbolic software such as *Maple*, it is possible to obtain general solutions to the differential equations in (15), but the obtained mathematical expressions are too complex to be displayed here. Instead, as a demonstration, the simplified version of the equations in (16) are solved, and the obtained general solutions are used to construct shape functions.

The general solutions to (16) are obtained as

$$\begin{cases} u(x) = c_7 + c_8\,x \\ v(x) = c_1 + c_2\,x + c_3\,x^2 + c_4\,x^3 \\ w(x) = c_9 + c_{10}\,x + c_{11}\,x^2 + c_{12}\,x^3 \\ \varphi(x) = c_5 + c_6\,x \\ \theta(x) = (c_2 - \frac{6\,EI_y}{k\,GA}) + 2\,c_3\,x + 3\,c_4\,x^2 \\ \psi(x) = (-c_{10} + \frac{6\,EI_z}{k\,GA}) - 2\,c_{11}\,x - 3\,c_{12}\,x^2 \end{cases} \tag{17}$$

where the twelve coefficients c_1, c_2, $\cdots$, c_{12} can be expressed with element nodal unknowns, u_1, v_1, $\cdots$, ψ_2, by enforcing the following element 'boundary conditions',

$$\begin{cases} u(0) = u_1, & v(0) = v_1, & w(0) = w_1, & \varphi(0) = \varphi_1, & \theta(0) = \theta_1, & \psi(0) = \psi_1 \\ u(L) = u_2, & v(L) = v_2, & w(L) = w_2, & \varphi(L) = \varphi_2, & \theta(L) = \theta_2, & \psi(L) = \psi_2 \end{cases} \tag{18}$$

After solving the algebraic equations resulted from the above conditions, the element field functions are now approximated as

$$\begin{cases} u = N_1 u_1 + N_2 u_2 \\ v = H_{v_1} v_1 + H_{\theta_1} \theta_1 + H_{v_2} v_2 + H_{\theta_2} \theta_2 \\ w = H_{w_1} v_1 + H_{\psi_1} \psi_1 + H_{w_2} w_2 + H_{\psi_2} \psi_2 \\ \varphi = N_1 \varphi_1 + N_2 \varphi_2 \\ \theta = G_{v_1} v_1 + G_{\theta_1} \theta_1 + G_{v_2} v_2 + G_{\theta_2} \theta_2 \\ \psi = G_{w_1} w_1 + G_{\psi_1} \psi_1 + G_{w_2} w_2 + G_{\psi_2} \psi_2 \end{cases} \tag{19}$$

where the element shape functions $N_1(\xi)$, $N_2(\xi)$, $\cdots$, $G_{\psi_2}(\xi)$ have the following expressions,

$$\begin{cases} N_1 = 1 - \xi \\ N_2 = \xi \\ H_{v_1} = \beta_y \left(2\xi^3 - 3\xi^2 + \alpha_y \xi + 1 - \alpha_y\right) \\ H_{v_2} = \beta_y \left(-2\xi^3 + 3\xi^2 - \alpha_y \xi\right) \\ H_{w_1} = \beta_z \left(2\xi^3 - 3\xi^2 + \alpha_z \xi + 1 - \alpha_z\right) \\ H_{w_2} = \beta_z \left(-2\xi^3 + 3\xi^2 - \alpha_z \xi\right) \\ H_{\theta_1} = L\beta_y \left[\xi^3 + (\frac{1}{2}\alpha_y - 2)\xi^2 + (1 - \frac{1}{2}\alpha_y)\xi\right] \\ H_{\theta_2} = L\beta_y \left[\xi^3 - (1 + \frac{1}{2}\alpha_y)\xi^2 + (\frac{1}{2}\alpha_y)\xi\right] \\ H_{\psi_1} = L\beta_z \left[\xi^3 + (\frac{1}{2}\alpha_z - 2)\xi^2 + (1 - \frac{1}{2}\alpha_z)\xi\right] \\ H_{\psi_2} = L\beta_z \left[\xi^3 - (1 + \frac{1}{2}\alpha_z)\xi^2 + (\frac{1}{2}\alpha_z)\xi\right] \\ G_{v_1} = \frac{6\beta_y}{L} \left(\xi^2 - \xi\right) \\ G_{v_2} = \frac{6\beta_y}{L} \left(-\xi^2 + \xi\right) \\ G_{w_1} = \frac{6\beta_z}{L} \left(\xi^2 - \xi\right) \\ G_{w_2} = \frac{6\beta_z}{L} \left(-\xi^2 + \xi\right) \\ G_{\theta_1} = \beta_y \left[3\xi^2 + (\alpha_y - 4)\xi + 1 - \alpha_y\right] \\ G_{\theta_2} = \beta_y \left[3\xi^2 - (\alpha_y + 2)\xi\right] \\ G_{\psi_1} = \beta_z \left[3\xi^2 + (\alpha_z - 4)\xi + 1 - \alpha_z\right] \\ G_{\psi_2} = \beta_z \left[3\xi^2 - (\alpha_z + 2)\xi\right] \end{cases} \tag{20}$$

with

$$\xi = \frac{x}{L}, \quad \alpha_y = \frac{12EI_y}{kGAL^2}, \quad \beta_y = \frac{1}{1 - \alpha_y}, \quad \alpha_z = \frac{12EI_z}{kGAL^2}, \quad \beta_z = \frac{1}{1 - \alpha_z} \tag{21}$$

In the above way, inter-dependence between element field functions is fully considered in the construction of shape functions. The obtained shape functions are thus consistent. Once element shape functions are constructed, it is straightforward to calculate element stiffness matrix. For uniform beam with symmetrical cross-section and linear elastic material, element stiffness matrix can be explicitly calculated with analytical integration. The explicitly derived expressions of element stiffness matrix for a three-dimensional 2-node Timoshenko beam element are provided in *Appendix A*.

4 Numerical Tests

The developed 3D 2-node Timoshenko beam element was tested with benchmarks to examine its immunity from shear locking and its performance in convergence. The obtained results are compared with those from the conventional isoparametric Timoshenko beam elements. The results produced by the developed Timoshenko beam element is denoted as $B3D2$ in the following figures. Exact and reduced integration are abbreviated as, respectively, 'E.I.' and 'R.I.' in the figures.

The cantilever beam shown in Fig. 3 was used in the test. The beam is clamped at its left end and affected by a shear force at its right end. The beam is made from isotropic, homogeneous material with Young's modulus

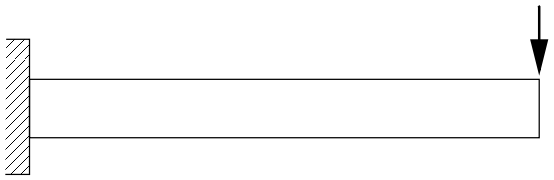

Figure 3: Cantilever beam under transverse force

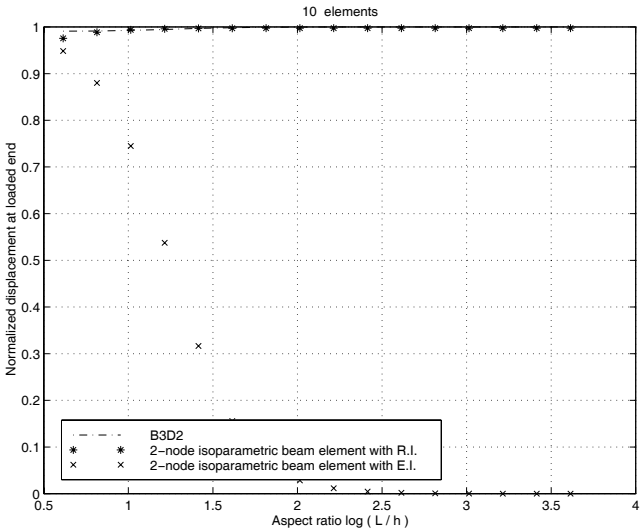

Figure 4: Immunity from shear locking test result

$E = 1.0MPa$ and Poisson's ratio $\nu = 0.3$. The first test was designed to test the immunity of shear locking. In the test, the beam was discretized using ten beam elements; all other parameters and conditions are fixed except beam

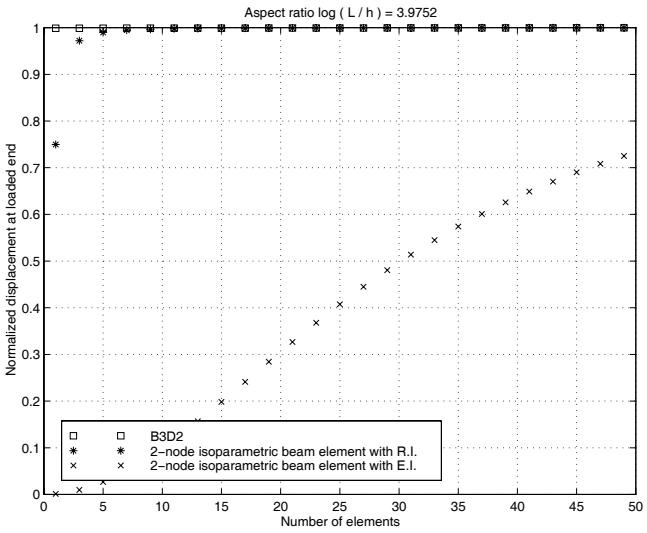

Figure 5: Convergence of developed 3D Timoshenko beam element

depth; The depth of the beam was gradually reduced so that the aspect ratio of the beam is becoming larger and larger. The aspect ratio of a beam is defined as the logarithm of the ratio between the beam length (L) and the beam depth (h), i. e., $log(\frac{L}{h})$. The obtained displacements at the right tip of the beam are normalized with analytical solutions and shown in Fig. 4. As expected, the conventional 2-node Timoshenko beam element with exact integration suffers from shear locking; therefore, the predicted deflection at the loaded tip becomes smaller and smaller with the beam becoming more and more slender. Although the use of reduced integration can greatly improve the situation, the performance of the element is still not optimal.

In the second test, the performance of the developed beam element in convergence was examined. In this test, all the parameters and conditions including the aspect ration of the beam were fixed, the number of beam elements used to simulate the beam was gradually increased. The obtained displacements at the loaded beam end are normalized by analytical solutions and displayed in Fig. 5. From the results, it can be observed that the convergence of the developed Timoshenko beam element is superior than the conventional Timoshenko beam element with reduced integration. It is not surprising that it can be observed from the results that using the developed Timoshenko beam element, one element can produce an exact solution, as the element shape functions are constructed from the analytical solutions of the homogeneous Euler-Lagrangian equations.

5 Concluding remarks

An efficient 3D 2-node Timoshenko beam element was developed. The shape functions of the element are constructed from the general solutions to the homogeneous Euler-Lagrangian equations. Numerical results show that the developed Timoshenko beam element is not only free from shear locking, but also has a superior convergence rate compared with its conventional isoparametric counterpart.

Appendix A

Explicit expressions of entries in the element stiffness matrix of a three-dimensional 2-node Timoshenko beam element, derived from consistent shape functions. The other entries that are not listed here are zeros.

$k_{1,1} = k_{7,7} = -k_{1,7} = \frac{EA}{L}$

$k_{2,2} = -k_{2,8} = \frac{12kGA\,EI_y(12EI_y+kGAL^2)}{L(12EI_y-kGAL^2)^2}$

$k_{2,6} = k_{2,12} = \frac{6kGA\,EI_y(12EI_y+kGAL^2)}{(12EI_y-kGAL^2)^2}$

$k_{3,3} = k_{3,9} = \frac{12kGA\,EI_z(12EI_z+kGAL^2)}{L(12EI_z-kGAL^2)^2}$

$k_{3,5} = k_{3,11} = -\frac{6kGA\,EI_z(12EI_z+kGAL^2)}{(12EI_z-kGAL^2)^2}$

$k_{4,4} = k_{7,7} = -k_{4,10} = \frac{G(I_y+I_z)}{L}$

$k_{5,5} = \frac{4EI_z[(kGA)^2L^4+3kGAL^2\,EI_z+36(EI_z)^2]}{L(12EI_z-kGAL^2)^2}$

$k_{5,9} = \frac{6kGA\,EI_z(12EI_z+kGAL^2)}{(12EI_z-kGAL^2)^2}$

$k_{5,11} = -\frac{2EI_z[72(EI_z)^2-(kGA)^2L^4-30kGAL^2\,EI_z]}{L(12EI_z-kGAL^2)^2}$

$k_{6,6} = \frac{4EI_y[(kGA)^2L^4+3kGAL^2\,EI_y+36(EI_y)^2]}{L(12EI_y-kGAL^2)^2}$

$k_{6,8} = -\frac{6kGA\,EI_y(12EI_y+kGAL^2)}{(12EI_y-kGAL^2)^2}$

$k_{6,12} = -\frac{2EI_y[-(kGA)^2L^4-30kGAL^2\,EI_y+72(EI_y)^2]}{L(12EI_y-kGAL^2)^2}$

$k_{8,8} = \frac{12kGA\,EI_y(12EI_y+kGAL^2)}{L(12EI_y-kGAL^2)^2}$

$k_{8,12} = -\frac{6kGA\,EI_y(12EI_y+kGAL^2)}{(12EI_y-kGAL^2)^2}$

$k_{9,9} = \frac{12kGA\,EI_z(12EI_z+kGAL^2)}{L(12EI_z-kGAL^2)^2}$

$k_{9,11} = \frac{6kGA\,EI_z(12EI_z+kGAL^2)}{(12EI_z-kGAL^2)^2}$

$$k_{11,11} = \frac{4EI_z[(kGA)^2L^4+3kGAL^2\,EI_z+36(EI_z)^2]}{L(12EI_z-kGAL^2)^2}$$

$$k_{12,12} = \frac{4EI_y[(kGA)^2L^4+3kGAL^2\,EI_y+36(EI_y)^2]}{L(12EI_y-kGAL^2)^2}$$

References

[1] R. Davis, R.D. Henshell, and G.B. Warburton. A Timoshenko beam element. *Journal of Sound and Vibration*, 22:475–487, 1972.

[2] Z. Friedman and J.B. Kosmatka. Improved two-node Timoshenko beam finite element. *Computers and Structures*, 47:473–481, 1993.

[3] A. W. Lees and D. L. Thomas. Unified Timoshenko beam finite element. *Journal of Sound and Vibration*, 80:355–366, 1982.

[4] Y. Luo. Field consistence approach with application to the development of finite element. In *The 10-th Nordic Conference on Computational Mechanics*, Tallinn, Estonia, 1997.

[5] Y. Luo. *On Shear Locking in Finite Elements*. KTH Bulletin (Licentiate Thesis), Stockholm, 1997.

[6] Y. Luo. Explanation and elimination of shear locking and membrane locking with field consistence approach. *Comput. Methods Appl. Mech. Engrg.*, 162:249–269, 1998.

[7] Y. Luo. *On Some Finite Element Formulations in Structural Mechanics*. KTH Bulletin (Doctorial Thesis), Stockholm, 1998.

[8] S. Mukherjee and G. Prathap. Analysis of shear locaking in Timoshenko beam elements using the function space approach. *Communications in Numerical Methods in Engineering*, 17:385–393, 2001.

[9] B. Nour-Omid and C.C. Rankin. Finite rotation analysis and consistent linearization using projectors. *Comput. Methods Appl. Mech. Engrg.*, 93:353–384, 1991.

[10] C. Pacoste and A. Eriksson. Beam elements in instability problems. *Comput. Methods Appl. Mech. Engrg.*, 144:163–197, 1997.

[11] J.N. Reddy. On locking-free shear deformable beam finite elements. *Comput. Methods Appl. Mech. Engrg.*, 149:113–132, 1997.

[12] T. Yokoyama. A reduced integration Timoshenko beam element. *Journal of Sound and Vibration*, 169:411–418, 1994.

Received: April 2, 2008